Permanent Magnet Bias, Homopolar Magnetic Bearings for a 130 kW-hr Composite Flywheel

Brian T. Murphy, Hamid Ouroua, Matthew T. Caprio, John D. Herbst
Center for Electromechanics, R7000, University of Texas, Austin, TX 78758
bmurphy@mail.utexas.edu

ABSTRACT

The Center for Electromechanics at the University of Texas at Austin is developing a power averaging flywheel battery for a high speed passenger locomotive as part of the Federal Railroad Administration's Next Generation High Speed Rail Program. The flywheel rotor, which weighs 5100 lb, is designed to store 130 kW-hr of energy at a top design speed of 15,000 rpm. The vertical rotor, which runs in a vacuum, is supported by a 5 axis magnetic bearing system. The flywheel housing is gimbal mounted to isolate the vehicle chassis from the gyroscopic forces in this dynamic application. A high speed 2 MW motor-generator, which is outside the vacuum, is directly coupled to the flywheel with the use of a rotary vacuum seal.

This paper discusses the design of the magnetic bearing actuators. There are two identical radial bearings and a double acting thrust bearing, each employing permanent magnet homopolar bias fields coupled with active control coils. The bearings employ permanent magnet homopolar bias fields. Some electromagnetic design analysis of the actuators is presented, along with test results for static electromagnetic fields measured within the bearing air gaps. Measured hysteresis loss in the radial bearing laminations is also presented. Analytical estimates of actuator bandwidth are compared to measurements.

A preliminary build of the flywheel rotor (the design of which is discussed in a companion paper) has been successfully spin tested to 13,600 rpm with the use of a digital bearing controller. Performance of the position sensors, fiber optic for radial and eddy current for axial, has thus far been adequate.

INTRODUCTION

The Federal Railroad Administration (FRA) is sponsoring development of an Advanced Locomotive Propulsion System (ALPS) for high speed passenger rail service. An overview of this project is given in [1] and [2]. Briefly, the propulsion system consists of a gas turbine directly coupled to a high speed generator. A flywheel battery directly coupled to a high speed motor/generator is used in conjunction with the turbine to provide power averaging. Compared to an all diesel-electric drive, the ALPS achieves significant reductions in size and weight, and offers improved fuel economy and reduced maintenance requirements.

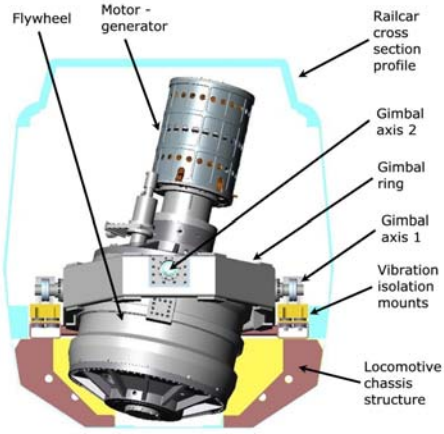

Figure 1. FRA-ALPS Flywheel battery.

At its heart, the flywheel battery (**Figure 1**) is a graphite epoxy composite rotor supported on magnetic bearings, and is described in detail in [3]. The topic of this paper is the magnetic bearing levitation system used to support the high speed flywheel rotor. The design of the actuators is described herein, along with various test results which focus on their electromagnetic performance.

The magnetic bearing system utilizes two identical radial bearings and a separate double acting thrust bearing. This basic topology is similar to that often used in magnetically levitated turbomachinery. However, this application is very different from turbomachinery applications because the rotor runs in a vacuum, and it is essential to minimize bearing power losses as much as possible. Therefore, all three bearings are of a homopolar design in that a steady bias flux is provided by a single pair of magnetic poles. These bias fields are generated by Neodymium Iron Boron rare earth permanent magnets in an effort to further increase system efficiency. The reference by Meeks, et al [4], describes this type of bearing topology in detail.

ACTUATOR DESIGN

Because this is such a demanding application, the design of the radial and axial actuators was an intensive effort. Among the key considerations are: required load capacity, vacuum environment and heat build up, spin stresses, dynamics of a relatively flexible flywheel rotor, and withstanding external disturbances from a moving vehicle. The preliminary design of the actuators was prepared by AVCON Inc., and was considered essentially complete when AVCON went out of business in the Summer of 1998. Although largely unchanged, a great many minor details of the actuator design were modified during final system design and fabrication.

The radial actuator design will be discussed first. **Figure 2** shows a cross section of a radial bearing. Some of the primary design parameters of this bearing are given in **Table 1**. Briefly, the stator has a single ring of permanent magnets in its midplane to provide a bias flux. There are 8 coils arranged in 4 quadrants. Each quadrant has a coil inboard and outboard of the permanent magnets. During detailed system analysis it was found necessary to drive each coil with its own power amplifier so as to overcome the relatively large inductance of the actuator. Thus the final design utilizes 4 power amplifiers for each radial control axis.

The required load capacity figure in **Table 1** is based on a "3 g" criteria, which is the specified vibration rating for all equipment mounted in the locomotive. This means the total capacity of both radial bearings together should be 3 times the weight of the rotor. Our present estimate of capacity is seen to be less than the 3 g target. This came about by the final rotor design being heavier than originally devised, and the increase in radial bearing air gap explained below.

The rotor laminations are thermally shrunk onto the hollow shaft. The 4340 shaft is part of the bias flux path of the homopolar bearing, and its inner and outer diameters are 2.5 and 5.8 inches, respectively. The fact that the shaft is hollow is an important feature enabling the rotor laminations to be assembled onto the shaft with an acceptable temperature delta, to remain tight on the shaft at all operating conditions, and with acceptable stresses. For the rotor 4130 was selected over M19 so as to maintain adequate fatigue life.

The dynamics of the ALPS flywheel rotor also require a significant contribution of bending stiffness from the laminations. Generally, rotor laminations offer little to no bending stiffness to help raise rotor flex mode natural frequencies. The rotor laminations are comprised of separate inboard and outboard stacks, with a solid ferrous (4340) spacer between them. The inboard stack was shrunk onto the rotor and held in a press with the 4340 spacer while both came to ambient temperature. The outboard stack was similarly mounted and pressed with a nonferrous Inconel 718 endplate. The 4340 and Inconel plates each have heavy interference on the shaft to act as "keepers", maintaining axial preload on the radial laminations.

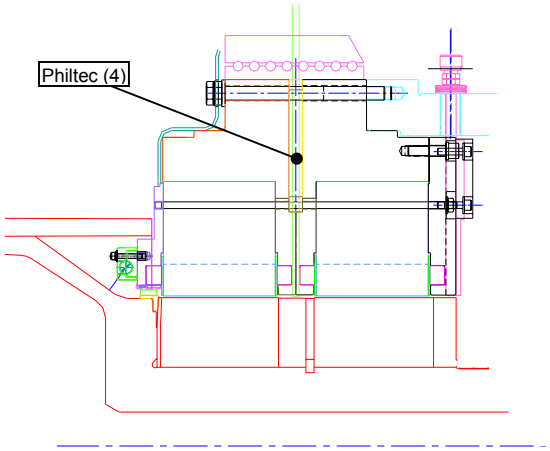

Figure 2. ALPS Radial magnetic bearing.

Table 1. Radial magnetic actuator parameters.

Load Capacity	6500 lb
Rotor Active Ax. Len.	10 inches
Rotor Diameter	11 inches
Radial Air Gap, ambient	0.060 inches
Radial Air Gap, hot	0.050 inches
Rotor Laminations	4130, 14 mil
Stator Laminations	M19, 14 mil
Displacement Sensors	Fiber Optic (4), Philtec Co-located at midplane
Bias Flux in Air Gap	0.9 Tesla
Coils	16 gauge copper wire 76*4 turns in each axis
Power supply	75 Volts 10/20 Amp cont/peak

Table 2. Stiffness versus air gap for radial bearing.

Air Gap (mils)	K bias (lb/mil)	K curr (lb/amp)
40	275	605.6
45	243	592.8
50	218	578.2
60	179	533.7
70	152	487.5

Figure 3 shows results of an axial compression test performed on a trial lamination stack. The goal was to achieve an effective 2 msi bending modulus on the flywheel. To help achieve the required axial compression, a set of wedges were pressed into a circumferential groove cut around the outer diameter at inboard end of each inboard stack. The 36 aluminum wedges in each bearing are held in place by an Inconel band shrunk over them (**Figure 2**).

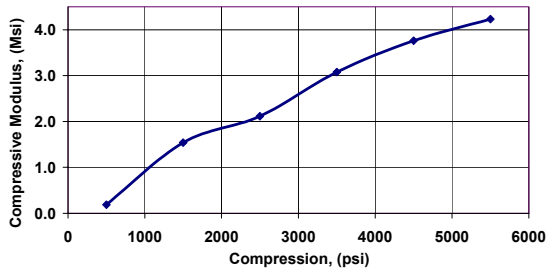

Figure 3. Results of axial compression test on a trial stack of 4130 14 mil laminations.

The fully assembled flywheel rotor is relatively flexible. The first flexible bending mode of the rotor is 20% above the maximum operating speed. Mainly because of this it was considered necessary to locate the radial displacement sensors at the bearing midplanes. Eddy current type sensors were not used over concerns of electromagnetic interference with the control coils and PWM style power amplifiers. The cleanliness of the vacuum environment of the flywheel enclosure led to the choice of fiber optic sensors from Philtec. These are reflection compensated devices with a useful linear range of about 5 mils to 70 mils of probe gap. Unfortunately, even though they are inherently low noise sensors, they have a small target spot size (about 0.125 inches) and high frequency response. This makes them prone to producing strong harmonic content up to very high harmonic numbers. Harmonic content is much higher than comparable eddy current sensors. Good signal quality requires a highly reflective and optically uniform rotor surface, free from blemishes. Our rotor surface is 4340 steel, which is subject to surface corrosion. After considering many possible surface treatments, and testing several, a white glossy high temperature engine paint was selected. In spin testing performed to date, the sensor/paint combination has performed adequately. This is in spite of a scratch that is believed to exist in the paint of one bearing. As expected, this scratch generates strong harmonics in the displacement feedback signal. In this particular instance the 5x component is quite strong and can be observed to excite system modes while running up in speed.

There are 4 sensors in each radial bearing at 90 degree spacing. The sensors are oriented parallel to the axes of the control coils. Opposing sensor pairs are differenced with an analog circuit to produce the feedback signal for its corresponding control axis (this also effectively cancels even numbered harmonics). All four sensors in each bearing are also averaged with an analog circuit to enable real time monitoring of changes in rotor diameter. During spin commissioning it was found beneficial to place an analog low pass filter at 32 kHz in each Philtec circuit to remove remnants of a carrier wave. This is because the combined analog signals exhibited beating due to small differences in the carrier wave frequency of individual sensors.

The original AVCON design called for a 40 mil radial air gap. However, the final rotor design ended up being sufficiently flexible that a drop onto the backup bearings was predicted to result in an actuator rub. Along with this, thermal expansion and centrifugal growth of the rotor will decrease the air gap by nearly ten mils. To reduce the chance of a rub, the assembled air gap was increased to 60 mils, which then transitions to 50 mils as the rotor speeds up and heats up.

A cross section of the thrust bearing is shown in **Figure 4**. This bearing is double acting with a single stator piece sandwiched between two rotating runners. The original load capacity design target for this bearing was “4 g” (3g plus rotor weight). The eventual 15,000 lb figure is due to current limits of the power supplies. This was considered acceptable for the locomotive application due to the relatively benign dynamic environment in the vertical axis, and isolation provided by the floor mount.

There are no laminations in this bearing as it is impractical to laminate the runners. Fortunately, the flux field is predominantly uniform in a circumferential sense. Thus, hysteresis losses are assumed to be insignificant. One of the most challenging aspects in the design of this bearing is in the mounting of the thrust runners onto the shaft. Because the runners are so large, their centrifugal growth at 15,000 rpm makes it impractical to mount them directly onto the shaft. In addition, the outboard runner must be removable to facilitate assembly and disassembly of the machine. The solution was to mount them compliantly with a pair of arbor carriers as depicted in **Figure 4**. The axial natural frequency introduced by the axial compliance of these runners is over 500 Hz. This is acceptable given the low frequency response of this actuator due to its solid construction.

One of the complications introduced by use of a compliant mount is that the air gap changes appreciably with speed. At high speed, centrifugal growth causes the runners to angle inward towards the stator. The air gap clearance at the OD and ID decrease by 15.7 and 4.6 mils, respectively, from rest to 15,000 rpm. There are additional decreases in air gap of up to 2.5 to 3 mils from magnetic attraction forces. Thus, the bearing was built to have a uniform air gap of 50 mils at 15,000 rpm. So the bearing is fabricated and assembled with a larger and tapered air gap. Obviously, great precision was required in the fabrication of these runners. Also, at over 90 lbm each, their assembly onto the rotor must be precise and repeatable because of the affect on both air gap and rotor balance.

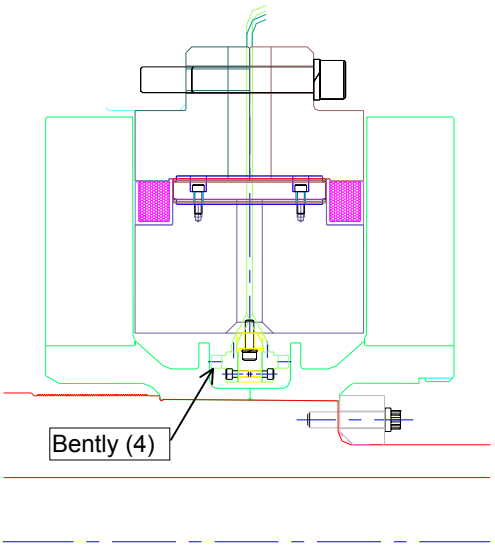

Figure 4. ALPS Thrust bearing actuator.

Table 3. ALPS Thrust Actuator Parameters.

Load Capacity	15,000 lb
Actuator Axial Length	8 inches
Runner Outer Diameter	16.5 inches
Axial Air Gap, Ambient	0.060 inches
Axial Air Gap, Spinning	0.050 inches
Runner Material	4340 Alloy Steel
Displacement Sensors	Eddy curr. (4), Bently
Bias Flux in Air Gap	0.67 Tesla
Coils	14 gauge copper wire 88 turns in 2 coils
Power supply	160 Volts 25/50 Amp cont/peak

Table 4. Thrust bearing stiffness versus air gap.

Air Gap (mils)	K bias (lb/mil)	K curr (lb/amp)
40	401	1041.3
50	317	806.7
60	262	660.0

The axial displacement sensors are eddy current type from Bently Nevada, and are located as shown in **Figure 4**. To fit in the limited space these are special 90 degree "button" style sensors. The sensors are mounted in two opposing pairs. The pairs are mounted 180 degrees from one another. The 4 signals are combined with an analog circuit to cancel synchronous runout as well as centrifugal and thermal changes in sensor gap. Dedicated axial target surfaces are incorporated into the thrust disk arbors to minimize the impact of flex on the measurement.

ELECTROMAGNETIC ANALYSIS

An electromagnetic analysis of the ALPS magnetic bearings was performed using the 3d and 2d finite element codes Opera-3d and Opera-2d from Vector Fields [5]. The 3d FEA model of the radial magnetic bearings, with their different components and corresponding materials, is shown in **Figure 5**. The model was constructed to reflect the actual bearings as-built, and this is a nonlinear model in that it accounts for actual B/H curves and saturation. The 3d flux distribution in the bearing is shown in **Figure 6** under the action of bias field and 1200 A-t in all the coils of one control axis. A profile of the bias field in the air gap around the circumference of the bearing at the center of one lamination stack is shown in **Figure 10**. Curves of force versus DC current for the radial bearings are shown in **Figure 11**. The bearings have a resultant current sensitivity of 534 lb/amp for the nominal assembled radial air gap of 60 mils.

The force output of the radial bearing was calculated for three different frequencies: 25 Hz, 50 Hz, and 250 Hz, in addition to DC. In this analysis eddy currents were allowed in the rotor spacer, shaft, rotor laminations, and pole pieces. Stator and rotor laminations were modeled as anisotropic materials, and currents flow in the planes of the laminations only. A single turn coil with a sinusoidal current waveform

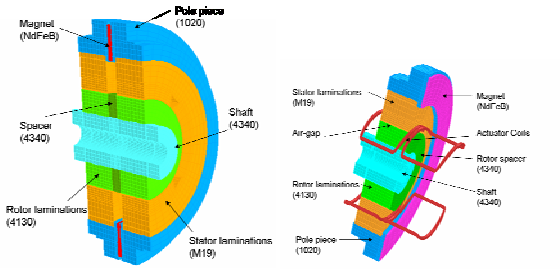

Figure 5. FEA model of radial bearing, ½ and ¼.

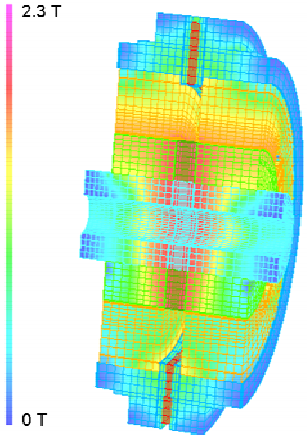

Figure 6. 3D Flux distribution for the radial bearing with bias field and 1200 A-t coil current.

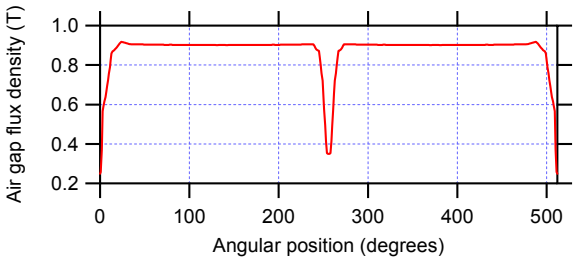

Figure 10. Circumferential distribution of radial bearing flux density in air gap at lamination stack mid-plan.

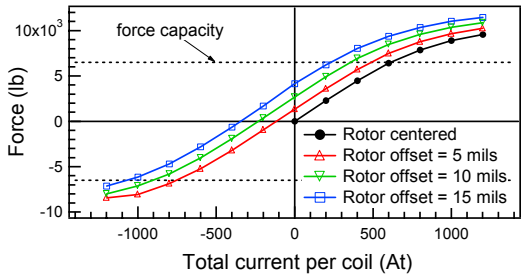

Figure 11. Radial bearing force versus current for one control axis with 40 mil air gap.

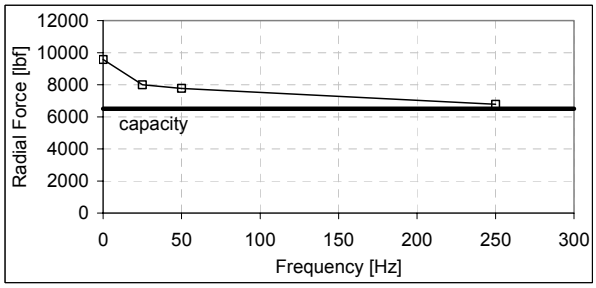

Figure 12. Frequency response of radial bearings.

representing 1200 A-t was used. These calculations were performed with the nominal clearance (0 rpm). **Figure 12** shows the radial force as a function of frequency. The force capacity drops relative to the static force by 17%, 19%, and 28% for the three frequencies. However, up to 250 Hz the radial bearings still achieve a force capacity of 6500 lb each.

A quarter FEA model of the thrust bearing is shown in **Figure 7**. **Figure 8** shows that the force versus DC current is quite linear up to 1200 A-t, which is close to the maximum available current. Shown later in **Figure 15**, an AC analysis predicts that at frequencies of 5 Hz, and 15 Hz, the force capacity drops by 63% and 76% respectively. The thrust bearings AC response is much more limited than that of the radial bearings because all materials in the thrust bearing are solid and conducting (no laminations).

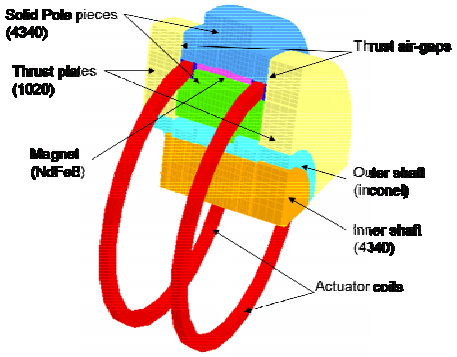

Figure 7. 3D FEA quarter model of thrust bearing.

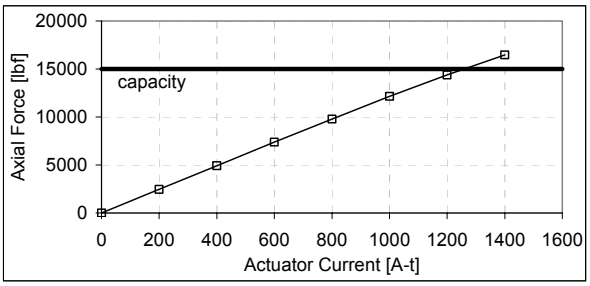

Figure 8. Force versus current for thrust bearing with 40 mil air gap.

TEST RESULTS

When the flywheel rotor was first levitated and rotated by hand we were surprised at the amount of drag exhibited. A number of slow roll spin down tests were conducted by spinning the rotor by hand to 15 rpm, and measuring the spin down with a 180 tooth wheel (**Figure 9**). Results clearly imply a constant net drag torque of approximately 8 in-lb. This was considerably higher than initially estimated. We had conservatively estimated the torque to be 1.8 in-lb with M19. Loss data for 4130 obtained on another project at UT-CEM indicated that 4130 was relatively close to M19. A constant torque should result with negligible windage and eddy current effects, and with no vacuum seal present. It was also interesting to see that when the rotor would come to a stop after a spin down, it would oscillate several times before finally becoming motionless. The rotor static position within the air gap was varied to see what affect it would have on the torque, both radially and axially. Minimum torque was

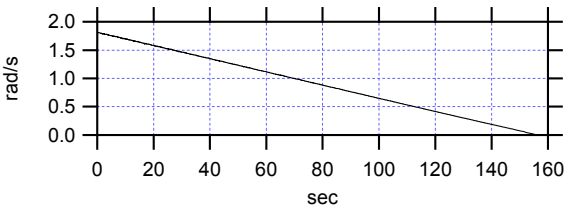

Figure 9. Spin down test of levitated flywheel from 15 rpm.

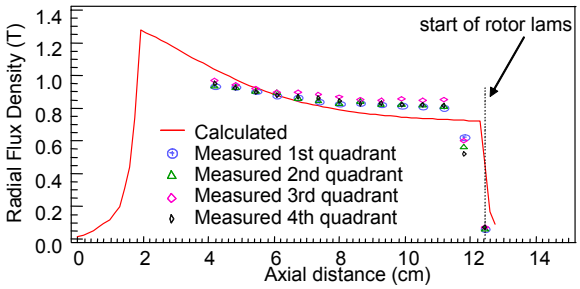

Figure 13. Measured and predicted bias flux density in the radial bearing air gap.

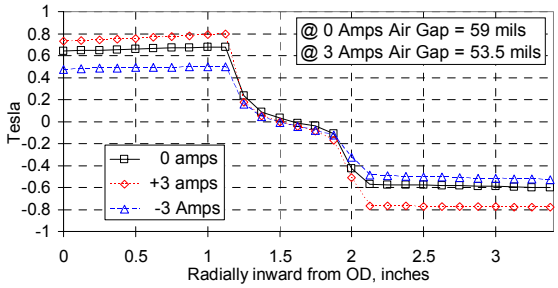

Figure 14. Measured flux in thrust bearing air gap.

found to correspond with the position of minimum coil current, which should be the "magnetic center" of the actuators. In the thrust axis minimum coil current is achieved with the rotor about 9 mils "high" so that the permanent magnets carry the rotor weight. Moving 10 mils away from center radially increased the measured drag torque by 17 percent, and moving 5 mils axially had no effect.

Hysteresis drag is a constant torque effect [6], and it can also create a spring like effect to cause the oscillations that were seen. **Figure 16** shows results of a B/H measurement of the 4130 rotor lamination material, and compares it to M19. This data now enables the prediction of the 8 in-lb of measured hysteresis drag torque. Unfortunately, however, this equates to 1.4 KW of losses directly on the rotor at 15,000 rpm, in addition to eddy current and windage losses. Whereas preliminary analysis predicted rotor heating would permit continuous operation, we now expect operation at high speed to be time limited. To test this, the rotor was run continuously for 8 hours at 5000 rpm. Rotor surface temperature was measured with an infrared thermocouple on the conical rotor surface just inboard of the radial bearings. **Figure 17** shows the steady rise in temperature during the run. It is planned to repeat this test at higher speed, and it may prove necessary to switch to M19 laminations, in effect trading fatigue life for thermal performance.

A Hall probe sensor was inserted into the air gap of one radial bearing with the rotor mechanically constrained in a centered position. This flux density measurement is compared to predictions from the 3D

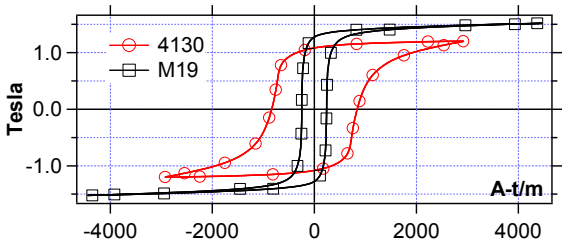

Figure 16. Measured B/H data for 4130, 14 mil thick, laminations.

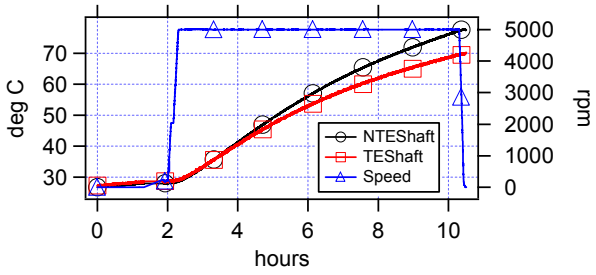

Figure 17. Measured temperature rise on rotor near one radial bearing during 8 hour run at 5000 rpm.

Vector Fields model in **Figure 13**. The comparison shows good agreement. **Figure 14** shows a similar measurement of the thrust bearing made by moving the sensor radially inward.

An area of concern with the thrust bearing is its limited frequency response given the solid construction. In many applications the thrust direction does not require nearly as high a frequency response as does the radial. In the dynamic environment of a locomotive the thrust bearing will be expected to react to dynamic inputs up to about 25 Hz. This limit comes about from the use of elastomeric isolation mounts to support the flywheel inside the locomotive. The mounts will be selected to give the machine a mounted natural frequency of 15 Hz so as to be above the fundamental flexible modes of the locomotive typically in the range of 5 to 10 Hz. The Vector Fields model of the thrust bearing was used to predict the load response of the actuator at 5 Hz and 15 Hz. To test for this, we again constrained the rotor in a centered position, and applied current to the thrust bearing coils at frequencies from 0 up to 15 Hz. The rotor constraint is not perfectly rigid, so we measured axial deflection with the actuator's position sensors. The measured deflection is taken as

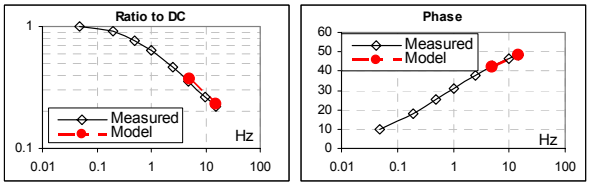

Figure 15. Measured and predicted frequency response of the thrust bearing.

an indicator of actuator force. Normalizing the dynamic deflection to the static deflection allows direct comparison to the analysis predictions. **Figure 15** compares the measured and predicted normalized load response versus frequency. The test results confirm that the frequency response is quite limited, and that the FEA model can be used to predict it.

A dynamic response analysis of the flywheel rotor and its housing to base motion input from the locomotive has been conducted. Actual worst case acceleration measurements taken on the floor of a locomotive running on the TTCI test track in Pueblo, Colorado were used as input for the analysis. At this time results are preliminary, but do indicate that the present thrust actuator has sufficient frequency response to handle the dynamic environment of a train.

SUMMARY

The design and electromagnetic analysis of the FRA-ALPS magnetic bearing actuators has been described in detail. Various test results used to anchor the analytical work have also been presented. The bearings have been fully fabricated, assembled and installed into the ALPS flywheel battery. The flywheel and its magnetic levitation system are currently undergoing spin commissioning. Maximum speed attained to date is 13,600 rpm (maximum operating speed is 15,000 rpm).

ACKNOWLEDGEMENTS

This material is based upon work supported by Federal Railroad Administration cooperative agreement, DTFR53-99-H-00006 Modification 4, dated April 30, 2003. Any opinions, findings, and conclusions or recommendations expressed in this publication are those of the authors and do not necessarily reflect the view of the Federal Railroad Administration and/or U.S. DOT.

REFERENCES

1 Herbst, John D. , Caprio, Matthew T., Advanced Locomotive Propulsion System (ALPS) Project Status 2003, Proceedings of IMECE '03: 2003 ASME International Mechanical Engineering Congress & Exposition, Washington D.C., November 16-21, 2003

2 Herbst, J. D. , Caprio, M. T., and Thelen, R. F., 2 MW 130 kWh Flywheel Energy Storage System, Electrical Energy Storage - Applications and Technology (EESAT2003), October 27-29, 2003, San Francisco, CA.

3 Caprio, Matthew T., Murphy, Brian T. and Herbst, John D., Spin Commissioning and Drop Tests of a 130 kw-hr Composite Flywheel, ISMB-9, August 3-6, 2004.

4 Meeks, C.R., DiRusso, E., Brown, G.V. , 1990, Development of a Compact, Light Weight Magnetic Bearing, AIAA/SAE/ SME/ASEE 26th Joint Propulsion Conference, Orlando, FL.

5 Vector Fields Inc., 1700 N.Farnsworth Ave., Aurora, IL 60505.

6 Kasarda, M., Allaire, P., Norris, P., Mastrangelo,, C., Maslen, E., Experimentally Determined Rotor Power Losses in Homopolar and Heteropolar Magnetic Bearings, IGTI, 1998, 98-GT-317.